Chinese Journal of
POLYMER SCIENCE

RESEARCH ARTICLE

https://doi.org/10.1007/s10118-026-3571-3
Chinese J. Polym. Sci.

Interface-engineered Ionically Conductive Polyoxometalate-based Hydrogels with High Stretchability and Notch-insensitivity for Wearable Sensors

Xiao-Jiao Shi, Yu-Bin Zhang, Na Li, Yu-Xuan Qiao, Ya Liang, Gong-Kuo Yu, Ai-Hong Su, Ze-Cheng Song, Dan-Dan Song, Ti-Feng Jiao*, and Zhi-Hui Qin*

State Key Laboratory of Metastable Materials Science and Technology, Hebei Key Laboratory of Applied Chemistry, Hebei Key Laboratory of Nanobiotechnology, Hebei Key Laboratory of Heavy Metal Deep-Remediation in Water and Resource Reuse, Yanshan University, Qinhuangdao 066004, China

Electronic Supplementary Information

Abstract The rapid advancement of wearable sensors necessitates ionically conductive hydrogels that simultaneously exhibit high stretchability, damage tolerance, and reliable adhesion. However, achieving these properties in a single material remains a significant challenge. Herein, we report an ionically conductive polyoxometalate (POM)-based hydrogel (PAA/L-arg@SIW) fabricated by incorporating L-arginine (L-arg)-modified silicotungstic acid nanocomplexes (L-arg@SIW) into a poly(acrylic acid) (PAA) network as a multifunctional dynamic crosslinker. Strong electrostatic interactions and hydrogen bonding between rigid L-arg@SIW nanoclusters and flexible PAA chains generate a three-dimensional hard-soft synergistic network, in which dynamic crosslinks preferentially rupture and re-form under mechanical loading, thereby dissipating energy and suppressing crack propagation. Consequently, the hydrogel exhibits exceptional stretchability (fracture strain >1500%), high toughness (1483 kJ/m^3), outstanding crack resistance (fracture energy up to 6.82 kJ/m^2), and high ionic conductivity (0.15 S/m), along with robust adhesion to diverse substrates. Hydrogel-based sensors demonstrate high strain sensitivity (gauge factor (GF)=8.06), fast response, and excellent cyclic stability, enabling reliable monitoring of human motion and high-fidelity acquisition of electrocardiogram (ECG) and electromyogram (EMG) signals. This study presents an effective strategy for constructing high-performance ionically conductive hydrogels for wearable sensing applications.

Keywords Hydrogel; High stretchability; Notch-insensitivity; Self-adhesion; Wearable sensor

Citation: Shi, X. J.; Zhang, Y. B.; Li, N.; Qiao, Y. X.; Liang, Y.; Yu, G. K.; Su, A. H.; Song, Z. C.; Song, D. D.; Jiao, T. F.; Qin, Z. H. Interface-engineered ionically conductive polyoxometalate-based hydrogels with high stretchability and notch-insensitivity for wearable sensors. *Chinese J. Polym. Sci.* https://doi.org/10.1007/s10118-026-3571-3

INTRODUCTION

Flexible wearable bioelectronic devices that can conformally interface with soft biological tissues and continuously acquire mechanical or electrophysiological signals have attracted increasing attention for applications in health monitoring,[1,2] human-machine interfaces,[3,4] and intelligent rehabilitation.[5,6] As core functional components, flexible wearable sensors are highly valued for their excellent deformability and signal transduction capability, enabling real-time transduction of joint motions, muscle contractions, and bioelectrical activities into readable electrical outputs.[7] However, during practical operation, such sensors are inevitably subjected to large tensile strains, repeated bending, and complex multiaxial loading. Under these conditions, pre-existing or load-induced defects within the bulk material or at the surface can readily initiate and accelerate crack propagation, ultimately leading to the mechanical failure and distortion of the acquired signals.[8] Therefore, the development of soft functional materials that simultaneously exhibit high stretchability, toughness, and resistance to crack propagation is essential for achieving reliable, long-term wearable sensing.

Recently, ionically conductive hydrogels have been widely regarded as promising soft functional materials for strain sensors, owing to their high water content, tissue-like mechanical compliance, and tunable ionic conductivity.[9,10] Nevertheless, conventional single-network conductive hydrogels generally have two intrinsic limitations. First, the relatively low polymer chain density and lack of effective energy-dissipation mechanisms result in intrinsic brittleness, limited extensibility, and insufficient toughness.[11] Second, once microcracks or notches are present, severe stress concentration at the crack tips under external loading can readily induce rapid through-thickness fracture, dramatically shortening the fatigue lifetime and severely undermining operational reliabili-

* Corresponding authors, E-mail: tfjiao@ysu.edu.cn (T.F.J.)
E-mail: zhqin@ysu.edu.cn (Z.H.Q.)
Special Topic: Functional Gels
Received December 29, 2025; Accepted January 12, 2026; Published online April 16, 2026

ty.[12] Considerable efforts have been devoted to addressing these challenges through structural design (*e.g.*, double-network architectures[13] and slide-ring crosslinking[14]), compositional engineering (*e.g.*, incorporation of nanofillers[15,16]), and modulation of crosslinked mechanisms (*e.g.*, introduction of diverse reversible sacrificial bonds[17]). Although these strategies enhance the strength and toughness to varying degrees, many systems remain highly defect-sensitive, exhibiting pronounced reductions in the fracture strain and fracture energy in the presence of notches or scratches.[8] Additionally, some toughening strategies based on rigid fibers[18] or highly dense crosslinked networks[13] often compromise softness and large deformability, which conflicts with the requirements of wearable devices. More critically, although mechanical reinforcement has been extensively explored, maintaining or enhancing stable and efficient ionic conductivity—crucial for high-fidelity strain sensing and low-impedance bioelectronic interfaces—remains largely underexplored.[19] Consequently, developing hydrogels that concurrently exhibit high stretchability, high toughness, robust crack-propagation resistance, and good ionic conductivity remains a major challenge in flexible wearable bioelectronics.

Among the emerging strategies to improve the comprehensive performance of conductive hydrogels, incorporating inorganic nanoscale building blocks with strong interfacial coupling and multifunctional crosslinking capabilities has proven particularly promising.[20] In this context, polyoxometalates (POMs) have attracted considerable interest owing to their well-defined molecular structures, high charge density, and designable metal-oxygen cluster architectures.[21–23] On one hand, the oxygen-rich surfaces of POMs can form dynamic crosslinking networks with positively charged or polar group-containing polymers and small molecules *via* electrostatic interactions and hydrogen bonding.[24,25] On the other hand, their low proton dissociation energy and continuous proton-hopping sites impart excellent proton or ionic conductivity, allowing simultaneous mechanical reinforcement and ionic conduction.[26] Despite these advantages, most reported POM-based composite hydrogels treat POMs merely as rigid fillers, with interfacial interactions limited to weak physical adsorption and loose cross-linked structures.[27,28] This often results in poor dispersion, discontinuous energy-dissipation pathways, and insufficient resistance to crack propagation, particularly under notched or large deformation conditions. Therefore, designing POM-based functional units capable of forming strong yet dynamic interfacial crosslinks with polymer networks through molecular- and nanoscale interface engineering, thereby constructing ionically conductive hydrogels with high toughness and robust crack-propagation resistance, has emerged as a critical and unresolved challenge.

Herein, we report a POM-based ionically conductive hydrogel that employs L-arginine (L-arg)-modified silicotungstic acid nanocomplexes (L-arg@SIW) as dynamic multifunctional crosslinking centers. In this system, poly(acrylic acid) (PAA) serves as a flexible primary network, whereas L-arginine (L-arg), bearing protonated amino and guanidinium groups, and Keggin-type silicotungstic acid (SIW) are introduced into the aqueous phase, where they self-assemble into L-arg@SIW nanocomplexes *via* multiple electrostatic interactions and hydrogen bonding and are subsequently uniformly embedded within the PAA network. The rigid L-arg@SIW nanoclusters, interconnected with flexible PAA chains through abundant dynamic ionic and hydrogen bonds, construct a robust hard-soft synergistic network that preferentially fractures under mechanical stress to dissipate energy efficiently, thereby significantly suppressing crack propagation. Owing to this "multisite anchoring and dynamic reconstruction" interfacial coupling mechanism, the resulting PAA/L-arg@SIW hydrogel exhibits a combination of outstanding properties, including high stretchability (fracture strain of 1572%), high toughness (1483 kJ/m^3), and pronounced resistance to crack propagation (fracture energy up to 6.82 kJ/m^2), together with high ionic conductivity (0.15 S/m) arising from continuous proton-conduction pathways provided by SIW. Furthermore, the hydrogel exhibited a strong adhesion to various substrates. Leveraging these properties, the PAA/L-arg@SIW hydrogel functions not only as a flexible strain sensor capable of accurately capturing multi-scale human motions, from subtle facial and throat movements to large joint bending, but also as a flexible bioelectrode for stable monitoring of electrophysiological signals, such as electrocardiograms (ECG) and electromyograms (EMG). Overall, this study demonstrates that rational molecular design that enables synergistic coupling between POMs and polymer networks offers a generalizable strategy for developing highly ionically conductive hydrogels with exceptional softness, toughness, and crack resistance, providing a robust material platform for flexible electronics, health monitoring, and human-machine interaction applications.

MATERIALS AND METHODS

Materials

Acrylic acid (AA, 99%), silicotungstic acid ($H_4SiW_{12}O_{40}$, ≥99.9%), L-arginine (98%), and ammonium persulfate (APS, 98%) were supplied by Aladdin Co., Ltd. (Shanghai, China). All the chemicals were used as received without further purification.

Fabrication of PAA/L-arg@SIW Hydrogels

The PAA/L-arg@SIW hydrogel was synthesized using a one-pot polymerization strategy. The synthesis procedure is as follows. First, 0.059 g of L-arginine was dissolved in 3 mL of ultrapure water under magnetic stirring for 10 min until a clear solution was obtained. Subsequently, 0.246 g of silicotungstic acid (SIW) was added and the mixture was stirred vigorously for an additional 10 min to form a homogeneous solution. Next, 1.779 g of acrylic acid (AA) monomer was introduced and stirred for 10 min to ensure thorough mixing. Subsequently, 0.0089 g of ammonium persulfate (APS, 0.5 wt% relative to the mass of AA) was added as the thermal initiator, followed by continuous stirring for 5 min. The resulting solution was then ultrasonicated for 30 s to remove entrapped air bubbles. Finally, the precursor solution was poured into a mold and thermally polymerized at 60 °C for 6 h to obtain a PAA/L-arg@SIW hydrogel. A series of hydrogel samples was prepared by systematically varying the total mass fraction of L-arginine and SIW, their molar ratio, and the mass fraction of AA to evaluate structure-property relationships. The detailed compositions of the prepared hydrogels are sum-

https://doi.org/10.1007/s10118-026-3571-3

marized in Table S1 (in the electronic supplementary information, ESI). Unless otherwise stated, the PAA/L-arg@SIW hydrogel prepared with a total mass fraction of L-arginine and SIW of 6 wt%, a molar ratio of 4:1, and an AA content of 35 wt% was used for subsequent performance evaluation.

CHARACTERIZATION

General Characterizations

Fourier transform infrared (FTIR) spectroscopy (Nicolet IS10) was used to characterize the chemical structures of the individual components and hydrogels over the wavenumber range of 400–4000 cm^{-1}. The microstructures of the freeze-dried hydrogels were examined by scanning electron microscopy (SEM, S-4800II). The molecular structures of the hydrogels were further analyzed by Raman spectroscopy (Horiba Jobin Yvon XploRA PLUS). The optical absorbance and transmittance of the hydrogels were measured using a UV-Vis spectrophotometer (UV-2550).

Mechanical Tests

Mechanical tests were conducted at room temperature using a universal testing machine equipped with a 100 N load cell. For uniaxial tensile and cyclic loading-unloading tests, the PAA/L-arg@SIW hydrogels were cut into standard dumbbell-shaped specimens (35 mm × 2 mm × 1 mm). A constant tensile rate of 50 mm/min was applied, and each test was repeated at least thrice to ensure data reproducibility. The elastic modulus was determined from the slope of the linear region of the stress-strain curve within a strain range of 0%–50%, whereas the toughness was calculated by integrating the area under the entire tensile stress-strain curve. Energy dissipation was quantified from the area enclosed by the loading-unloading hysteresis loops. For the compression tests, cylindrical PAA/L-arg@SIW hydrogel samples with a diameter of 8 mm and a height of 10 mm were prepared, and both single and cyclic compression tests were conducted at a constant crosshead speed of 5 mm/min.

Fatigue Tests

The fracture energies of the hydrogel samples were measured using the single-edge notched tensile (SENT) method. Rectangular SENT specimens (10 mm × 1 mm, initial crack length 2 mm) were subjected to uniaxial tensile testing on a universal testing machine (AGS-X, Shimadzu, Japan) at a crosshead speed of 5 mm/min, while the corresponding stress-strain curves were recorded. All tests were conducted at room temperature and were repeated three times to ensure reproducibility. In addition, specimens featuring circular, linear, and triangular notches were prepared and tested at various tensile rates. The fracture energy (Γ) was calculated using the following equation:

$$\Gamma = \frac{6Wc}{\sqrt{\lambda}} \tag{1}$$

where c is the notch length, W is the area under the stress-strain curve from the initial state to the fracture strain of the intact specimen, and λ is the elongation at fracture of the notched specimen.

Adhesion Tests

The interfacial adhesion of the PAA/L-arg@SIW hydrogel was evaluated using a lap shear test. Hydrogel strips with identical dimensions were prepared and sandwiched between two substrate pieces, including paper, glass, pig skin, PET, silicone rubber, PMMA, stainless steel, and copper. Gentle pressure was applied for approximately 5 min to ensure intimate contact and sufficient bonding. The adhered assemblies were subsequently stretched on a universal testing machine at a crosshead speed of 50 mm/min until complete separation of the substrates. Adhesive strength was calculated by dividing the maximum load at failure by the initial bonded area.

Electrical and Sensing Tests

The electrical conductivity of the PAA/L-arg@SIW hydrogels was characterized by electrochemical impedance spectroscopy (EIS) using an electrochemical workstation (CHI760E, CH Instruments, China). Rectangular hydrogel samples were sandwiched between two copper electrodes and connected to a workstation to obtain the AC impedance spectra. Conductivity (σ, S/m) was calculated using the following equation:

$$\sigma = \frac{L}{R \times S} \tag{2}$$

where L (m) denotes the length of the ionogel sample, S (m^2) and R (Ω) indicate the cross-sectional area and resistance of the ionogel, respectively.

The sensing behavior of the PAA/L-arg@SIW hydrogel was evaluated by coupling a universal testing machine with an LCR meter. The relative change ($\Delta R/R_0$) was calculated as follows:

$$\frac{\Delta R}{R_0} = \frac{R - R_0}{R_0} \tag{3}$$

where R and R_0 denote the instantaneous resistance under deformation and initial resistance in the undeformed state, respectively.

The gauge factor (GF) was defined as:

$$\mathrm{GF} = \frac{\Delta R/R_0}{\varepsilon} \tag{4}$$

where ε denotes the applied strain. Response and recovery times were obtained by stretching the hydrogel to 50% strain at a stretching rate of 240 mm/min. All the tests were conducted under ambient laboratory conditions of approximately (25±5) °C and 40%–60% relative humidity. During conductivity measurements, the samples were enclosed in self-sealing bags to reduce water loss. For sensing performance tests, a thin layer of vacuum silicone grease was applied to the hydrogel surface to effectively suppress dehydration and the associated degradation of the sensing performance.

For human motion monitoring, the assembled hydrogel-based wearable sensors were conformally attached to various body sites such as the face, throat, wrist, and knee. The corresponding sensing signals were recorded using an LCR meter (E4980AL; Keysight).

Skin impedance was determined by placing the hydrogel working electrode and reference electrodes on the flexor side of the forearm with an interelectrode distance of 40 mm. Each electrode had an effective contact area of approximately 78 mm^2. For electrocardiogram (ECG) measurements, two hydrogel patches were placed on the left and right forearms as the working and reference electrodes, respectively, and an additional hydrogel electrode was fixed on the right lower leg and used as the ground. A similar configuration was employed to assess the electromyography (EMG) monitoring capability of

the hydrogel electrodes. The working and reference electrodes were attached to the right arm to capture EMG signals between the two sites, whereas the ground electrode was placed on the left arm to minimize motion artifacts during muscle contraction. ECG and EMG signals were synchronously acquired using a multichannel physiological signal acquisition system (RM6240XC). For all strain-sensing tests and physiological signal measurements, the PAA/L-arg@SIW hydrogel was directly adhered to the skin owing to its intrinsic adhesiveness, and no additional tape was applied over the active sensing region. Before attachment, the skin was gently wiped with an alcohol pad and allowed to dry to remove sweat and skin oils. Outside the sensing area, lead wires were connected to the hydrogel electrodes using conductive tape and then secured to the skin with insulating tape. No additional conductive paste was used in the tests. Each measurement was completed within several minutes under ambient laboratory conditions to minimize the influence of sweat and sebum.

RESULTS AND DISCUSSION

Fabrication and Structural Analysis of L-arg@SIW Nanocomplex-crosslinked PAA Hydrogel

The fabrication and network structure of the PAA/L-arg@SIW hydrogel are shown in Fig. 1(a). First, L-arginine and SIW were pre-assembled in water *via* electrostatic interactions and hydrogen bonding to form L-arg@SIW nanocomplexes. Acrylic acid (AA) and the thermal initiator ammonium persulfate (APS) were subsequently added, and the mixture was polymerized at 60 °C for 6 h to yield the PAA/L-arg@SIW hydrogel. Acting as rigid nano-crosslinkers, L-arg@SIW interacted extensively with the flexible PAA chains through electrostatic and hydrogen bonds, significantly enhancing the mechanical performance of the hydrogel. Meanwhile, the intrinsic high proton mobility of the SIW endowed the hydrogel with excellent ionic conductivity, making it suitable for wearable sensors capable of detecting human motion and physiological signals (Fig. 1b).

FTIR spectroscopy confirmed the formation of the L-arg@SIW nanocomplexes and their tight integration into the PAA network (Fig. S1 in ESI and Fig. 1c). As shown in Fig. S1 (ESI), the characteristic Si—O, W=O, and W—O—W vibrations of SIW at 1015, 977, 906, and 741 cm^{-1} were retained in L-arg@SIW, but shifted to 974, 927, and 796 cm^{-1}.[26,29] Simultaneously, the N—H stretching of L-arginine shifted from 3048 cm^{-1} to 3280 cm^{-1}, while the carboxylic C=O absorption weakened, and a new band appeared at 1636 cm^{-1}.[30,31] These results indicated that L-arginine cations and SIW anionic clusters formed a strongly coupled L-arg@SIW nanocomplex through cooperative electrostatic interactions and hydrogen bonding.[32] In the PAA/L-arg@SIW hydrogel, the C=C stretching of AA at 1635 cm^{-1} disappeared (Fig. 1c), confirming the successful PAA backbone formation.[33] Meanwhile, the C=O stretching band of the carboxyl group in AA at 1698 cm^{-1} and the bending vibration of $-NH_3^+$/guanidinium N—H and partial $-COO^-$ at 1636 cm^{-1} merged into a sharper C=O absorption at 1704 cm^{-1}, and the O—H stretching of PAA red-shifted from 3088 cm^{-1} to 3056 cm^{-1}, indicating dense hydrogen-bonding and electrostatic interactions between PAA chains and L-arg@SIW. [26,34] Notably, the Keggin-type SIW bands at 974 and 927 cm^{-1} shifted to 966 and 922 cm^{-1}, suggesting reconfiguration of the electronic environment and ionic coordination around the SIW clusters.[26] Raman spectroscopy further corroborated the crosslinked interactions in the PAA/L-arg@SIW hydrogel (Fig. S2 in ESI). The W=O vibration of SIW at 984 cm^{-1} and the guanidinium band of L-arginine at 1321 cm^{-1} were clearly observed, verifying the incorporation of both components. The PAA C—C/C—O backbone vibration shifted from 1079 cm^{-1} to 1092 cm^{-1}, reflecting local chemical environment changes induced by coupling with L-arg@SIW nanocomplexes.[35–37] Together, these results demonstrate that L-arg@SIW nanocomplexes were successfully integrated into the PAA network through multiple noncovalent interactions, forming a dynamic, mechanically robust supramolecular network.

SEM was used to investigate the internal crosslinking structure and assess the influence of L-arg@SIW on the microstructure of the PAA/L-arg@SIW hydrogel. The pure PAA hydrogel exhibited a porous structure with relatively large pores and loose network (Fig. S3 in ESI). In contrast, the PAA/L-arg@SIW hydrogel displayed significantly smaller, more uniformly distributed pores and a denser, continuous network, indicating that L-arg and SIW cooperatively formed L-arg@SIW nanocrosslinking points, reinforcing interchain connections and increasing the effective crosslinking density (Fig. 1d). Simultaneously, the EDS elemental maps of C, O, and W exhibited a homogeneous spatial distribution across the hydrogel matrix, confirming that the L-arg@SIW nanocomplexes were uniformly embedded in the PAA network. This rigid nanocluster-flexible polymer chain synergy efficiently distributes and dissipates stress over a larger volume. Despite its compact structure, the PAA/L-arg@SIW hydrogel maintained a high visible-light transmittance (about 92%, Fig. 1e), comparable to that of pure PAA, indicating uniform nanoscale dispersion without macroscopic phase separation and excellent optical compatibility.

Mechanical Toughness and Crack-propagation Resistance of the PAA/L-arg@SIW Hydrogel

The mechanical properties of the pure PAA, PAA/L-arg, PAA/SIW, and PAA/L-arg@SIW hydrogels were comparatively investigated by uniaxial tensile testing (Figs. 2a and 2b). The pure PAA hydrogel exhibited a relatively poor tensile performance, with a fracture stress of 70.6 kPa and a fracture strain of 648% (Fig. 2a). Upon incorporation of SIW, the PAA/SIW hydrogel displayed a markedly enhanced fracture strain of 1236%, accompanied by a slight decrease in the fracture stress. This behavior can be attributed to the introduction of SIW, which partially weakened the direct interchain interactions between PAA chains and increased network flexibility, thereby improving the ductility. However, the relatively weak interfacial interactions between the SIW and PAA chains resulted in a slight reduction in tensile strength.[38] Owing to the strong hydrogen bonds and electrostatic interactions between the protonated amino groups ($-NH_3^+$) and guanidinium cations of L-arginine and the carboxylate group ($-COO^-$) of the PAA chains, the PAA/L-arg hydrogel exhibited both increased fracture stress (130.3 kPa) and fracture strain (763%). Furthermore, when L-arg@SIW nanocomplexes were introduced as robust and multifunctional dynamic physical crosslinking nodes uniformly embedded with-

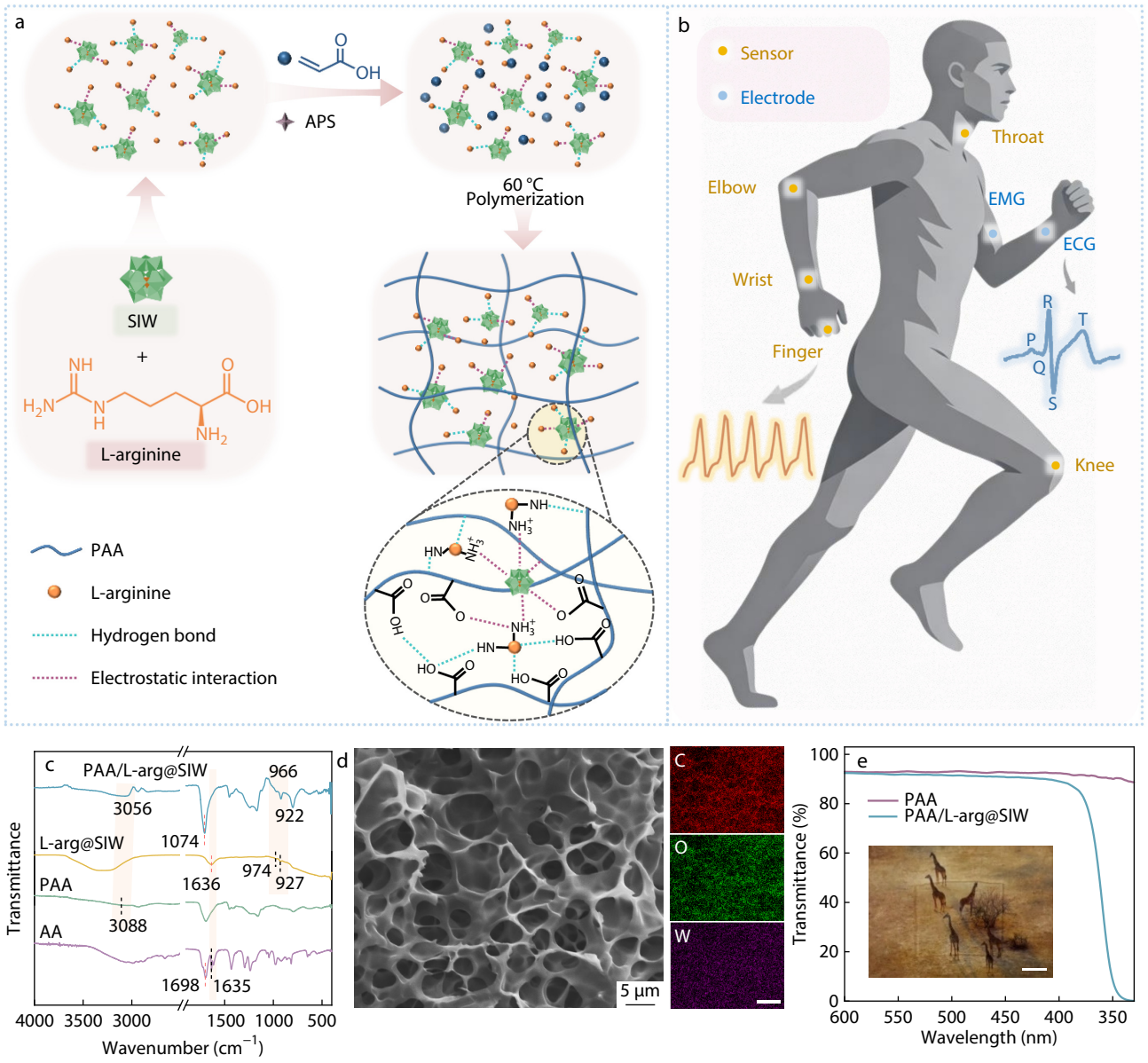

Fig. 1 Fabrication and characterization of the PAA/L-arg@SIW hydrogel. (a) Schematic illustration of the preparation of PAA/L-arg@SIW hydrogels; (b) Schematic of PAA/L-arg@SIW hydrogels used as flexible wearable sensors for monitoring various human activities; (c) FTIR spectra of AA, L-arg@SIW nanocomplex, PAA, and PAA/L-arg@SIW hydrogels; (d) SEM image of the PAA/L-arg@SIW hydrogel and EDS elemental mappings showing uniform distribution of C, O, and W (scale bar: 5 μm); (e) Transmittance spectra of PAA and the PAA/L-arg@SIW hydrogel in the visible region (scale bar: 1 cm).

in the PAA network, the PAA/L-arg@SIW hydrogel achieved the highest fracture stress (164.7 kPa) and strain (1572%), both of which were significantly higher than those of the PAA/SIW and PAA/L-arg hydrogels. In addition, the incorporation of L-arg@SIW significantly improved the toughness and elastic modulus of the hydrogel (Fig. 2b). The PAA/L-arg@SIW hydrogel exhibited a skin-like elastic modulus of 68.7 kPa together with a high toughness of 1483 kJ/m^3, exceeding those of pure PAA, PAA/SIW, and PAA/L-arg hydrogels. The outstanding mechanical performance may be attributed to the nano-reinforcement effect of SIW and the abundant interfacial bonding between SIW and PAA chains bridged by L-arg, which can effectively dissipate mechanical energy by the rupture of dynamic interfacial interactions and stress transfer between polymer chains *via* nanoscale stress-transferring centers.[39]

The L-arg/SIW molar ratio, total content, and AA content also play crucial roles in determining the mechanical properties of the hydrogels. As shown in Figs. S4 and S5 (in ESI), the elastic modulus remained relatively stable with increasing L-arg/SIW molar ratio and total content, whereas the tensile strength, fracture strain, and toughness reached their maximum values at an L-arg/SIW molar ratio of 4:1 and total content of 6 wt%. Meanwhile, the effect of AA content on the mechanical performance exhibited an initial increase followed by a decline. With the increase in AA content, the increased crosslinking density led to a pronounced enhancement in the

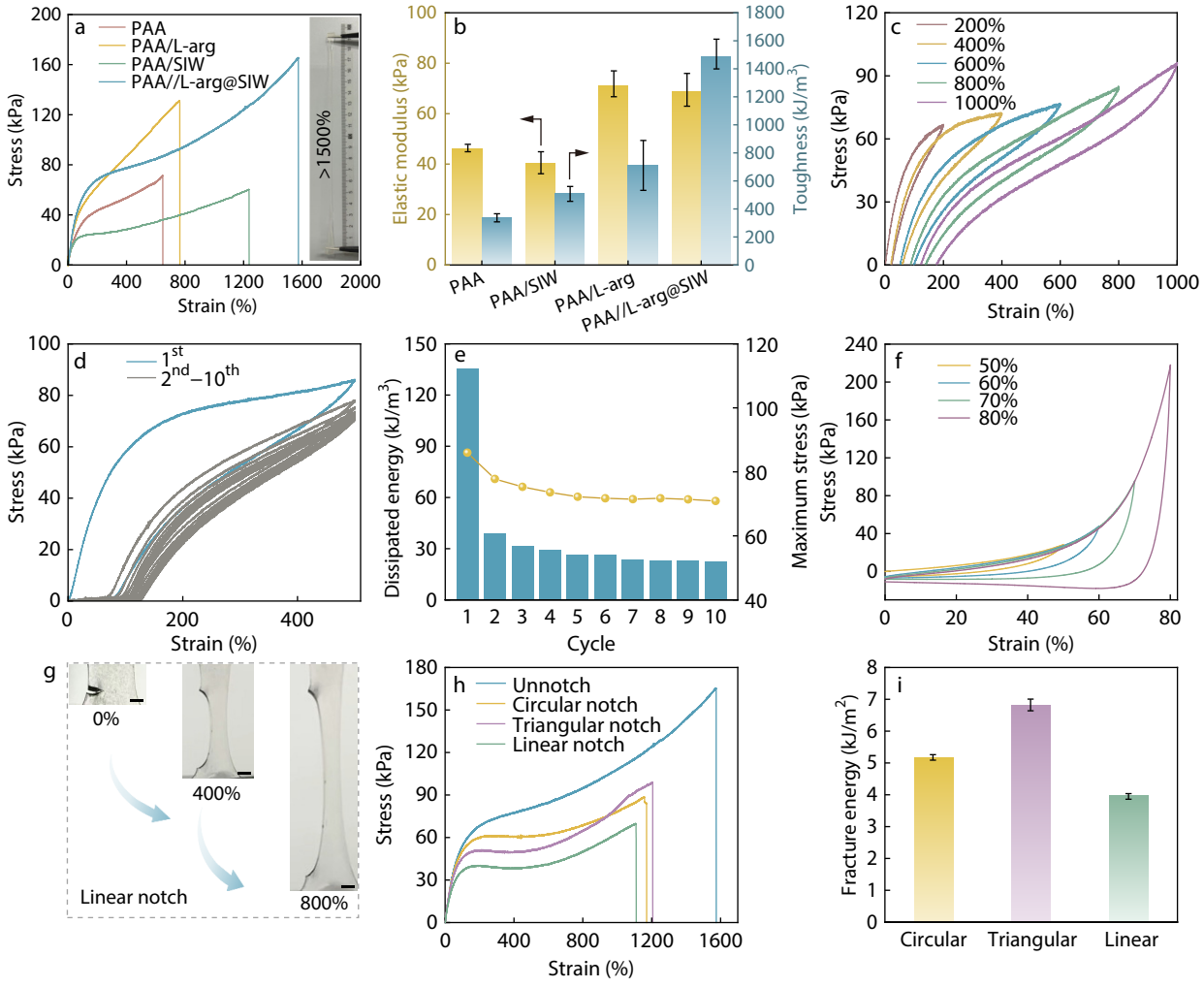

Fig. 2 (a) Tensile stress-strain curves and (b) the corresponding elastic modulus and toughness of the PAA, PAA/L-arg, PAA/SIW and PAA/L-arg@SIW hydrogels; (c) Cyclic loading-unloading tensile curves of the PAA/L-arg@SIW hydrogel at different maximum strains (200%, 400%, 600%, 800% and 1000%); (d) Ten successive cyclic tensile loading-unloading curves and (e) the corresponding dissipated energies and tensile stress of the PAA/L-arg@SIW hydrogel under 500% strain; (f) Cyclic loading-unloading compression curves of PAA/L-arg@SIW hydrogels at different maximum strains (50%, 60%, 70%, and 80%); (g) Optical photographs of the linear-notched PAA/L-arg@SIW hydrogel sample stretched perpendicular to the notch direction (scale bar: 2 cm); (h) Tensile stress-strain curves and (i) the corresponding fracture energies of the PAA/L-arg@SIW hydrogel samples with various notch shapes.

mechanical properties (Fig. S6 in ESI). However, at AA contents above 35 wt%, the fracture strain decreased slightly owing to the stress concentration caused by network densification.[40] Based on these results, a composition with an L-arg/SIW molar ratio of 4:1, total L-arg/SIW content of 6 wt%, and AA content of 35 wt% was selected as the optimal formulation for subsequent studies.

The energy dissipation capability and fatigue resistance of the PAA/L-arg@SIW hydrogel were systematically investigated through tensile loading-unloading tests. As shown in Fig. 2(c) and Fig. S7 (in ESI), both the hysteresis loop area and dissipated energy increased progressively as the applied strain increased from 200% to 1000%, indicating that an increasing number of dynamic crosslinking sites undergo reversible rupture under higher deformation to effectively dissipate mechanical energy. During ten consecutive loading-unloading cycles without rest intervals, the PAA/L-arg@SIW hydrogel exhibited excellent cyclic mechanical stability (Figs. 2d and 2e). The stress softening and residual deformation observed after the first loading-unloading cycle are mainly attributed to the rupture and rearrangement of relatively weak physical crosslinks within the initial network. Thereafter, the mechanical response rapidly reached a steady state, with both the tensile strength and dissipated energy remaining nearly constant throughout the subsequent cycles. The outstanding fatigue resistance and self-recovery behavior of the PAA/L-arg@SIW hydrogel originate from the reversible rupture and reformation of multiple dynamic physical crosslinks, including ionic interactions and hydrogen bonds, within the network. Upon loading, these dynamic noncovalent interactions preferentially dissociated to dissipate energy, thereby protecting the crosslinked PAA backbone from irreversible damage. Upon unloading, the dissociated ionic and hydrogen bonds rapidly reformed, driven by polymer chain relaxation, enabling efficient recovery of the network topology.[41] Notably, the L-arg@SIW nanocomplex crosslinking sites acted as

robust multifunctional nodes that preserved structural integrity under cyclic deformation and provided stable, well-defined topological anchoring points for dynamic bond reformation, ensuring the repeatability of the recovery process. The PAA/L-arg@SIW hydrogel exhibited remarkable compressive properties. As illustrated in Fig. S8(a) (in ESI), as the total content of L-arg and SIW increased from 0 wt% to 8 wt%, the compressive strength at 80% strain gradually increased from 119.8 kPa to 315.4 kPa, confirming the beneficial role of L-arg@SIW dynamic crosslinking points in enhancing the compressive load-bearing capacity. At various maximum strains, the compressive stress-strain curve displayed pronounced hysteresis loops, and the specimens nearly fully recovered their original shape after unloading (Fig. 2f), indicating that the PAA/L-arg@SIW hydrogel also possessed an efficient energy dissipation mechanism under compression. Furthermore, five consecutive compression cycles (Fig. S8b in ESI) revealed a relatively large hysteresis observed in the first cycle, whereas the subsequent hysteresis loops remained stable with minimal variation in dissipated energy, further confirming the durability and reliability of the PAA/L-arg@SIW hydrogel under cyclic compressive loading.

In soft materials, macroscopic fatigue damage and fracture failure are fundamentally governed by the initiation and progressive propagation of cracks under external loading driven by the severe stress concentration at the crack tip. Therefore, enhancing resistance to crack initiation and propagation is crucial for extending the service lifetime of soft functional materials.[42] Benefiting from the reinforcing effect of L-arg@SIW nanocomplexes, the PAA/L-arg@SIW hydrogel exhibited exceptional resistance to crack propagation. As shown in Fig. 2(g) and Fig. S9 (in ESI), when a pre-notched hydrogel specimen was subjected to uniaxial tension perpendicular to the crack direction, it could be stretched to strains exceeding 1000% without any observable advancement of the crack tip, directly demonstrating its excellent crack-propagation stability. As shown in Figs. 2(h), 2(i) and Movies S1–S3 (in ESI), hydrogels containing circular, triangular, and linear notches sustained ultimate strains of 1169%, 1206%, and 1107%, respectively, prior to failure, corresponding to fracture energies of 5.18, 6.82, and 3.96 kJ/m^2. In addition, the PAA/L-arg@SIW hydrogels with different notch shapes exhibited negligible strain-rate dependence, as evidenced by the nearly identical mechanical responses under various stretching rates (Fig. S10 in ESI), further confirming its robust resistance to crack propagation. The outstanding anti-crack propagation performance of the PAA/L-arg@SIW hydrogel originates from the function of the L-arg@SIW nanocomplexes as efficient stress transfer and energy dissipation centers within the polymer network. Through multiple dynamic ionic and hydrogen bonds formed between protonated amino/guanidinium groups and polyoxometalate clusters, the L-arg@SIW nanodomains tightly anchor multiple flexible PAA chains in the vicinity of rigid nanoclusters, forming local hard-soft synergistic microdomains. When stress is concentrated at the crack tip, these dynamic noncovalent interactions preferentially undergo reversible dissociation and reformation, enabling effective load transfer between the flexible polymer chains, while continuously dissipating mechanical energy through repeated bond-breaking processes. Consequently, the stress concentration at the crack tip was significantly alleviated, rapid crack penetration was strongly suppressed, and catastrophic fracture and structural failure of the hydrogel were effectively delayed.[43]

Adhesion Properties of the PAA/L-arg@SIW Hydrogel

In addition to its outstanding mechanical properties, the PAA/L-arg@SIW hydrogel exhibited an exceptional universal adhesive capability. As shown in Fig. 3(a), the hydrogel firmly adhered to a wide range of substrates under a 20 g load, including metals (copper and steel), inorganic materials (glass), cellulosic materials (paper and wood), and polymers (PET, PMMA, and silicone), highlighting its broad adaptability and applicability in complex interfacial environments. To evaluate the interfacial adhesion strength quantitatively, the adhesive performance of the PAA/L-arg@SIW hydrogel on different substrates was systematically characterized using lap shear tests (Fig. 3b). The adhesion strengths toward paper, pigskin, copper, glass, PET, steel, PMMA, and silicone were measured to be 56.42, 38.66, 39.59, 33.73, 28.12, 28.48, 20.01, and 9.04 kPa, respectively (Fig. 3c), demonstrating broad and substrate-independent adhesion compatibility across surfaces with diverse physicochemical characteristics, including hydrophilic/hydrophobic, rigid/flexible, and organic/inorganic interfaces.

Stable and reliable interfacial adhesion is essential for maintaining the long-term functional integrity of hydrogels under dynamic service conditions, particularly for sensing applications that require continuous signal output, where interfacial stability directly affects the signal fidelity and signal-to-noise ratio. Therefore, the adhesion durability of the PAA/L-arg@SIW hydrogel was evaluated using cyclic lap shear tests. As illustrated in Fig. 3(d), no noticeable degradation in adhesion strength was observed after eight successive loading-unloading cycles on the metal, skin, glass, and polymer substrates, indicating excellent antifatigue characteristics and interfacial recoverability. Furthermore, paper (hydrophilic and rough) and PET (hydrophobic and smooth) were selected as representative substrates with contrasting surface properties to investigate the time-dependent evolution of the adhesion strength. As shown in Fig. S11 (in ESI), the adhesion strength on paper exhibited only marginal variation, increasing by merely 6.56 kPa after 1 h of contact, suggesting rapid interfacial bonding and high interfacial stability. By contrast, the adhesion strength on PET increased significantly to 50.44 kPa over the same period. This contrast primarily originates from the distinct interfacial interaction mechanisms. The surface structure of the paper facilitates the rapid formation of a robust bond with the hydrogel *via* hydrogen bonding and mechanical interlocking. Conversely, the inert and smooth PET surface requires a longer time for the hydrogel to gradually establish tighter interfacial coupling through segment diffusion, rearrangement, and enhanced ion-dipole interactions, thereby resulting in a pronounced time-dependent strengthening effect.[44] This universal and resilient adhesion behavior can be ascribed to the synergistic design of the PAA/L-arg@SIW hydrogel in terms of modulus matching and chemical coupling (Fig. 3e). Specifically, the hydrogel possesses a soft tissue-like elastic modulus, allowing conformal contact with rough or irregular surfaces under low contact pressure.

https://doi.org/10.1007/s10118-026-3571-3

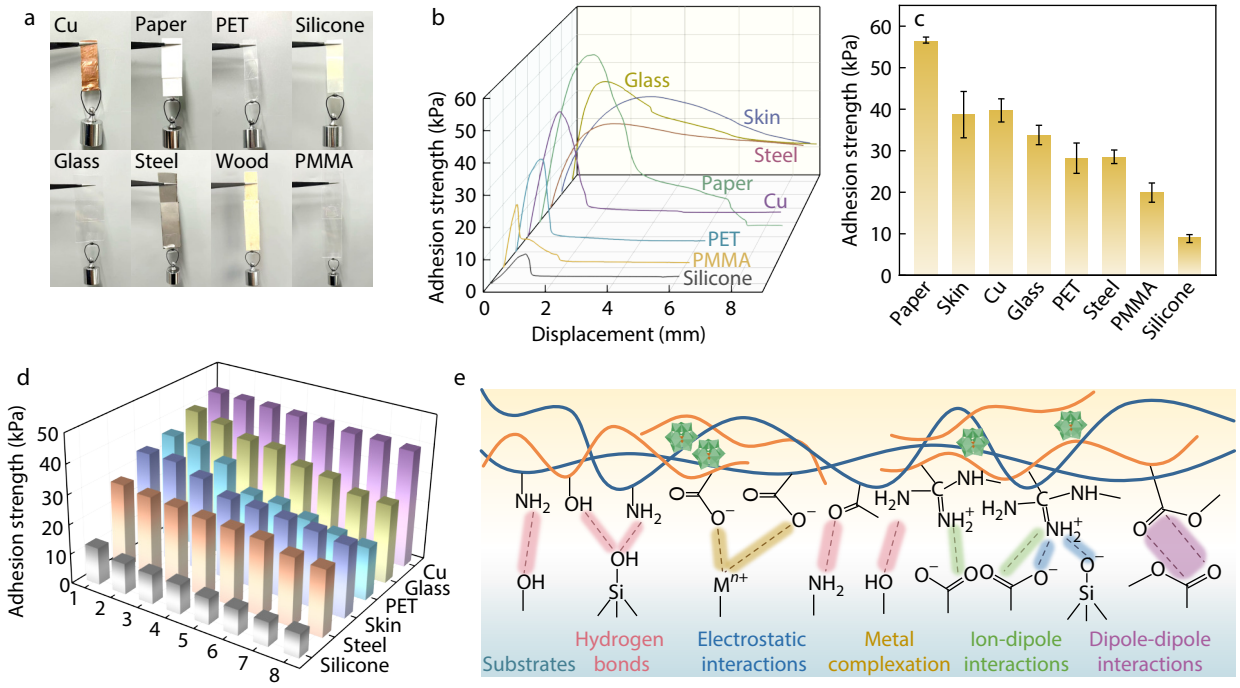

Fig. 3 Adhesion performance of the PAA/L-arg@SIW hydrogel. (a) Optical photographs of PAA/L-arg@SIW hydrogels adhering to various substrates (copper, steel, glass, paper, wood, PET, PMMA, and silicone) under load; (b) Representative lap-shear strength-displacement curves and (c) corresponding adhesion strength of the PAA/L-arg@SIW hydrogel on different substrates; (d) Adhesion strength over eight consecutive lap-shear cycles on skin, glass, metals, and polymers; (e) Schematic illustration of adhesion mechanisms between PAA/L-arg@SIW hydrogel and diverse substrates.

The network is enriched with multifunctional moieties, including carboxyl groups from PAA chains, protonated amino and guanidinium groups from L-arginine, and oxygen-rich coordination sites from SIW polyoxometalate clusters, which collectively enable strong yet dynamically reversible interfacial crosslinking with diverse substrates through multiple noncovalent interactions, such as hydrogen bonding, electrostatic attraction, coordination bonding, ion-dipole, and dipole-dipole interactions.[45,46] This multi-interaction adhesion strategy not only endows the hydrogel with broad adhesion applicability, but also establishes a robust material foundation for its practical implementation in bioelectronic interfaces, flexible sensing systems, and wearable devices.

Electrical and Sensing Properties of the PAA/L-Arg@SIW Hydrogel

Benefiting from the dynamic ion pairs formed between the protonated amino/guanidinium cations and polyoxometalate anions, a continuous and efficient ionic transport network was formed within the PAA/L-arg@SIW hydrogel. In this network, the electrostatic interactions between these ion pairs undergo continuous rearrangement and restructuring, offering abundant and stable pathways for directional ion migration through the polymer matrix. As a result, the PAA/L-arg@SIW hydrogel exhibited outstanding ionic conductivity, reaching 0.15 S/m (Fig. 4a), which is significantly higher than that of the control PAA, PAA/L-arg, and PAA/SIW hydrogels (0.02, 0.07, and 0.08 S/m, respectively). This substantial enhancement clearly illustrates the synergistic contribution of multiple components to the improvement in the ionic conduction.[46] When the PAA/L-arg@SIW hydrogel was integrated into a simple circuit containing an LED, the LED illuminated successfully, and its brightness changed synchronously and reversibly in response to the deformation of the hydrogel during cyclic stretching and release (Fig. S12 and Movie S4 in ESI), visually confirming the pronounced strain-dependent conductivity of the hydrogel and its real-time visual response to deformation.

To quantitatively assess the strain-sensing performance of the PAA/L-arg@SIW hydrogel, the real-time relative resistance variation ($\Delta R/R_0$) was monitored under uniaxial tensile loading, and the corresponding gauge factor GF (defined as the ratio of relative resistance change to applied strain) was subsequently determined.[47] As shown in Fig. 4(b), the $\Delta R/R_0$-strain curve is divided into three quasi-linear regimes with distinct slopes: GF of 1.58 in the low-strain region (0%–350%), GF of 4.33 in the medium-strain region (350%–1000%), and GF of 8.06 in the high-strain region (1000%–1572%). This segmented linear response suggests that the reconstruction of conductive pathways within the hydrogel network varies across deformation stages, from homogeneous stretching of the initially continuous network at low strain, to partial rearrangement of conductive paths at intermediate strain, and ultimately to pronounced elongation and restructuring of conductive channels at high strain. Such a multistage conduction evolution facilitates a wide range of highly sensitive detections, from small to ultra-large strains.[48] The response speed and signal stability of the PAA/L-arg@SIW hydrogel sensor were further evaluated through dynamic loading-unloading tests. At a strain of 50% and tensile rate of 240 mm/min, the sensor exhibited a rapid electrical response, with a response time of 149 ms and a recovery time of 380 ms

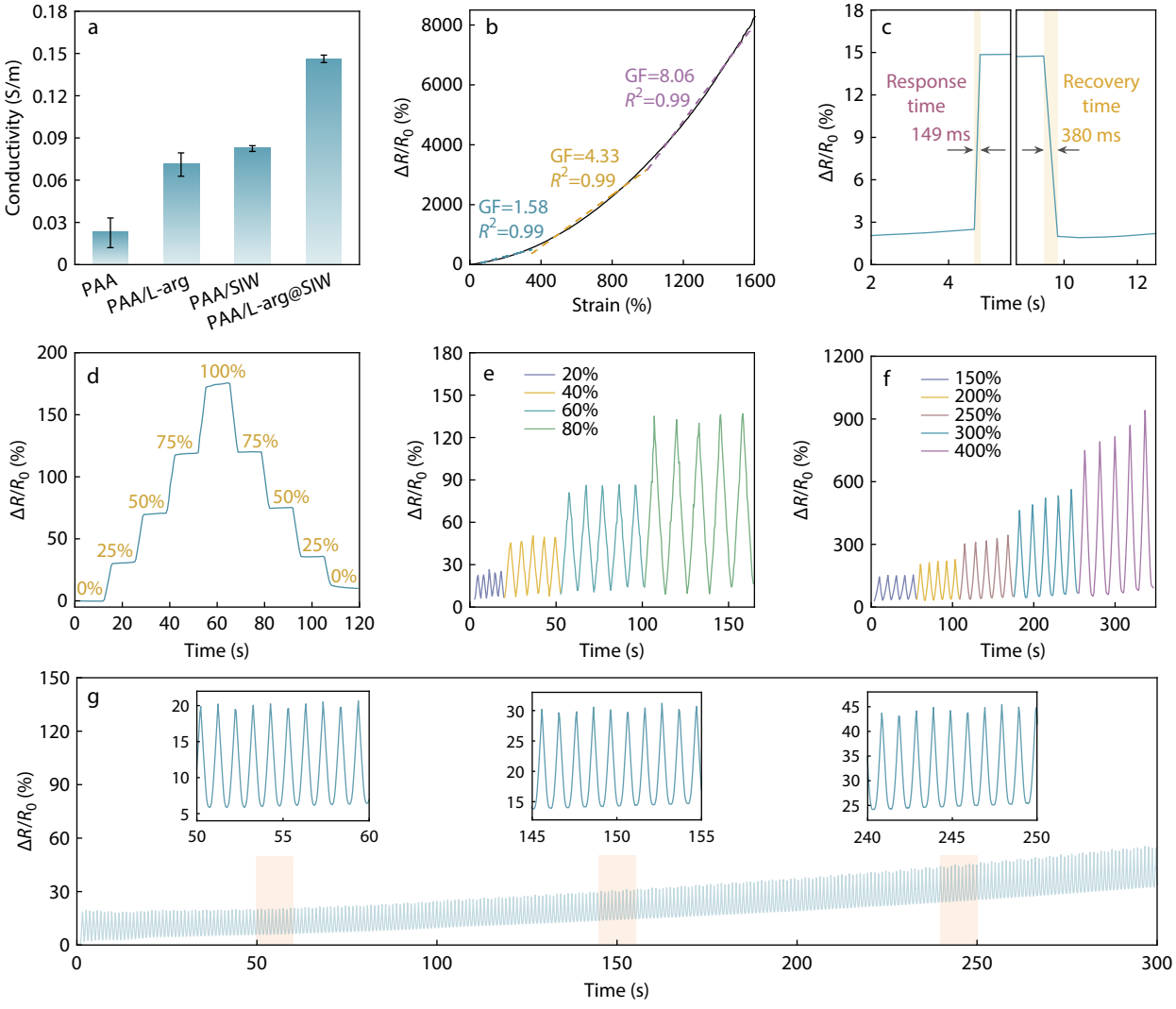

Fig. 4 Sensing performances of the PAA/L-arg@SIW hydrogel. (a) Ionic conductivity of PAA, PAA/L-arg, PAA/SIW, and PAA/L-arg@SIW hydrogels; (b) Relative resistance change ($\Delta R/R_0$) versus tensile strain of the hydrogel sensor and the corresponding GF; (c) Response and recovery time of the hydrogel sensor under instantaneous stretching-relaxation; (d) $\Delta R/R_0$ of the hydrogel during the stepwise increased strain from 0% to 100% and subsequent recovery. $\Delta R/R_0$ under stepwise cyclic stretching of (e) small strains (20%–80%) and (f) large strains (100%–400%); (g) Stability test of the hydrogel sensor under continuous stretching at 50% strain for 300 s.

(Fig. 4c). These results show that the hydrogel can rapidly establish a stable resistance change upon loading and revert to its initial electrical state upon unloading, reflecting its excellent capability for tracking dynamic deformation.

In addition, when the sensor was subjected to stepwise loading-unloading cycles between 0% and a maximum strain of 100%, the $\Delta R/R_0$ curves for each cycle segment nearly overlapped, confirming the high signal consistency and reliable cyclic performance (Fig. 4d). Moreover, the sensor exhibited robust dynamic recognition capability and stable output over a broad strain range. For small strain cycles (20%–80%, Fig. 4e), the $\Delta R/R_0$ signal smoothly followed the deformation continuously, with negligible hysteresis and noise. Under large strain cycles (150%–400%, Fig. 4f), despite the significantly increased deformation amplitude, $\Delta R/R_0$ still exhibited regular and periodic variations with well-defined strain dependence, indicating that the sensor remained stable and could effectively distinguish between different strain levels under severe deformation conditions. Notably, during a continuous stretching-releasing test at 50% strain for 300 s (Fig. 4g), the output of the sensor remained highly stable throughout the process, demonstrating excellent sensing durability and reliability. Taken together, these comprehensive performances, including high sensitivity, wide working range, fast response, good signal reproducibility, and long-term operational stability, satisfy the key requirements for strain-sensing materials in flexible and wearable electronics, positioning the PAA/L-arg@SIW hydrogel as a promising candidate for next-generation intelligent flexible devices and human-machine interaction systems.

Application as Wearable Sensors and Bioelectrodes

Owing to its excellent stretchability, high sensitivity, rapid response, and strong conformal adhesion, the PAA/L-arg@SIW hydrogel can be assembled into a flexible wearable sensor for the

https://doi.org/10.1007/s10118-026-3571-3

real-time monitoring of diverse human motions and physiological activities. As shown in Fig. 5(a), the sensor exhibited distinct response signals to varying finger-bending angles, with $\Delta R/R_0$ showing a stepwise increase at each bending angle (0°, 30°, 60°, and 90°), enabling the quantitative grading of joint flexion. During continuous finger bending (Fig. 5b), $\Delta R/R_0$ remained highly reproducible without response delay, confirming excellent cyclic stability and fast response. When attached to the wrist, each upward and downward motion produced distinct resistance peaks with varying amplitudes, enabling motion direction discrimination and reflecting the consistency of the bending cycles (Fig. 5c). Additionally, during elbow joint flexion-extension, the sensor outputs stable periodic signals synchronized with the joint angle changes (Fig. S13a in ESI), and similar results were observed during continuous knee bending (Fig. S13b in ESI), indicating reliable tracking of large-amplitude joint deformations and limb movements. For subtle motions, the sensor tracked facial and throat movements. As shown in Figs. 5(d) and 5(e), slight actions, such as cheek puffing and swallowing, induced distinct fluctuations in $\Delta R/R_0$. During cheek puffing (Fig. 5d), each inflation-deflation cycle caused a sharp increase and rapid recovery in the signal, demonstrating sensitivity to small skin deformations. For swallowing (Fig. 5e), the sensor produced regular, well-defined periodic waveforms that effectively detected subtle physiological activities. Finally, Fig. 5(f) shows the $\Delta R/R_0$ response to the slight pressing of the hydrogel, highlighting its fast response, stable cyclic waveforms, and suitability for tactile and pressure sensing.

The PAA/L-arg@SIW hydrogel exhibited excellent performance as a skin-interfacing bioelectrode for electrophysiological signal monitoring. The impedance spectra of the hydrogel and commercial Ag/AgCl electrodes were measured over a wide frequency range (0.1–10^5 Hz, Fig. 5g). The hydrogel electrodes exhibited significantly lower interfacial impedance, which was attributed to efficient ion-conducting pathways within the PAA/L-arg@SIW network and its excel-

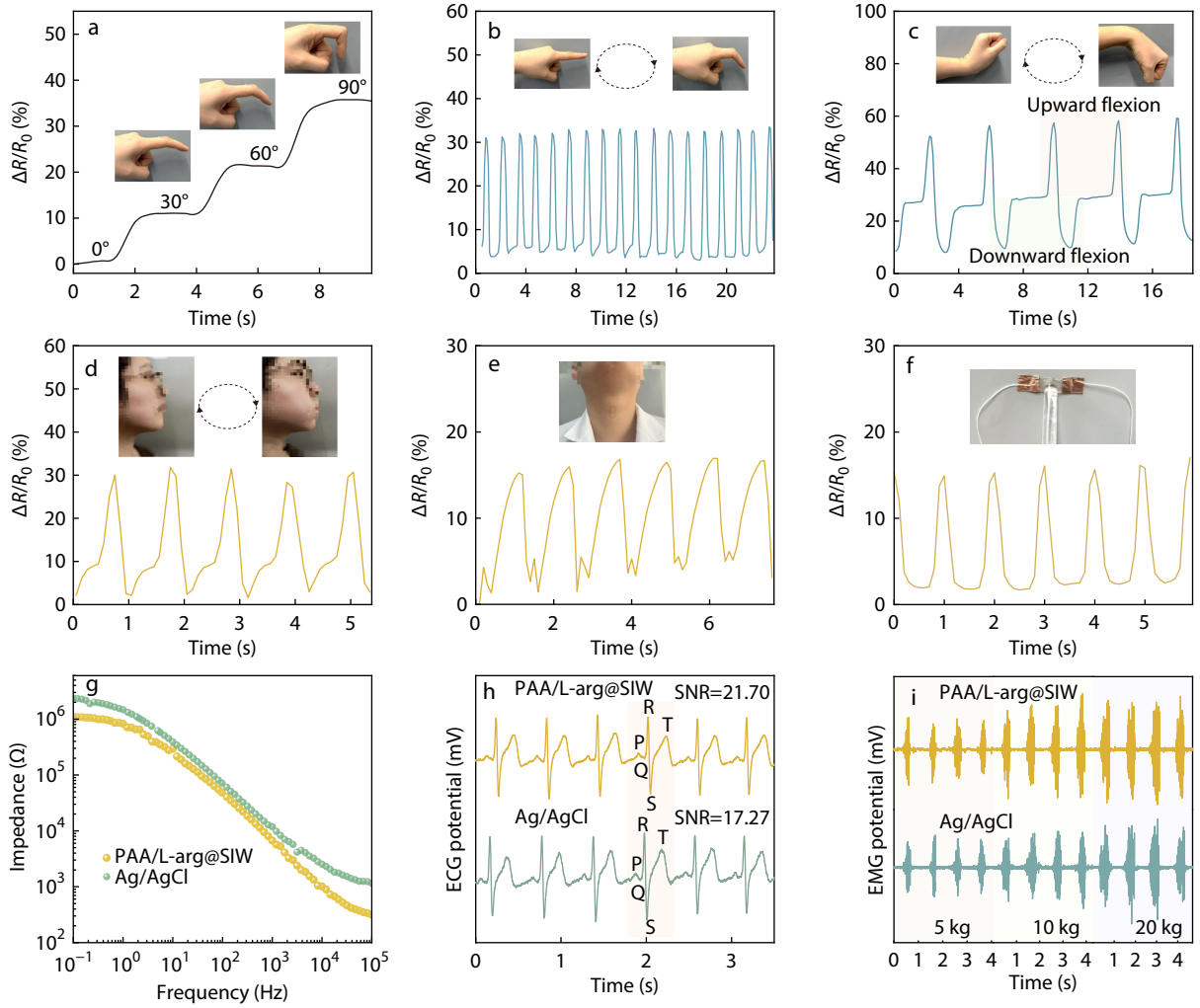

Fig. 5 Strain sensing and bioelectrodes applications of the PAA/L-arg@SIW hydrogel. Real-time response of the hydrogel sensor to multi-scale human motions: (a) stepwise finger bending at different angles (0° to 90°), (b) continuous finger bending-releasing cycles without interruption, (c) repetitive upward and downward wrist flexion, (d) cheek inflation, (e) swallowing, and (f) pressing. (g) Interfacial impedance spectra of PAA/L-arg@SIW hydrogel electrodes and Ag/AgCl electrodes on human skin; (h) ECG signals simultaneously captured by the hydrogel electrode and the commercial Ag/AgCl electrode; (i) Electromyogram (EMG) signals recorded by the hydrogel electrode and the Ag/AgCl electrode during periodic gripping-relaxation under different grip forces (5, 10, and 20 kg).

https://doi.org/10.1007/s10118-026-3571-3

lent conformal contact with the skin. On this basis, PAA/L-arg@SIW hydrogels were further employed as electrodes for recording electrocardiogram (ECG) and electromyogram (EMG) signals and were compared with commercial Ag/AgCl electrodes. Both electrodes clearly resolved the characteristic PQRST waveforms (Fig. 5h). However, the ECG signals collected by the hydrogel electrodes exhibited a flatter baseline and lower noise, and the corresponding signal-to-noise ratio (SNR=21.70) was notably higher than that of the Ag/AgCl electrodes (SNR=17.27), indicating a superior ECG acquisition quality under realistic skin conditions. Fig. 5(i) presents the EMG signals recorded at grip forces of 5, 10, and 20 kg. With increasing grip force, the amplitude of the EMG signals captured by the PAA/L-arg@SIW hydrogel electrodes increased accordingly, with well-defined contours and good inter-cycle reproducibility, enabling effective discrimination of different force levels, which was comparable to that of Ag/AgCl electrodes. Furthermore, when the hydrogel electrodes were attached to the forearm and upper arm muscles, EMG signals were recorded during the sustained lifting of dumbbells with different weights (1, 2.5, and 5 kg) (Fig. S14 in ESI). The results indicated that the peak amplitudes and waveform characteristics of the EMG signals under different loads were essentially consistent with those obtained using commercial electrodes, further confirming the practicality of the hydrogel electrodes for monitoring dynamic muscle activities. In summary, the PAA/L-arg@SIW hydrogel sensor can accurately and stably monitor multi-scale human motions and, as a hydrogel electrode, demonstrates outstanding performance in electrophysiological signal acquisition. These results highlight the PAA/L-arg@SIW hydrogel as a robust platform for multimodal flexible sensing systems in wearable health monitoring, human–machine interaction, and intelligent rehabilitation.

CONCLUSIONS

In summary, we developed a PAA/L-arg@SIW composite hydrogel that simultaneously achieved high toughness, outstanding resistance to crack propagation, and excellent ionic conductivity by employing L-arg@SIW nanocomplexes as dynamic crosslinkers. Strong electrostatic and hydrogen-bonding interactions between L-arginine and SIW enabled the construction of dynamically reconfigurable hard-soft synergistic crosslinking points within the flexible PAA network, giving rise to a multilevel energy dissipation mechanism dominated by reversible ionic bonds and hydrogen bonds. Benefiting from this structural design, the hydrogel exhibited a high fracture strain of 1572% and toughness of 1483 kJ/m^3, while maintaining remarkable defect tolerance and fatigue-resistant fracture behavior under different notch geometries and loading rates, with a fracture energy of 6.82 kJ/m^2. Meanwhile, the efficient proton transport pathways provided by the SIW endow the hydrogel with an ionic conductivity of 0.15 S/m. Moreover, the hydrogel exhibited strong adhesion to different matrices. The hydrogel-based sensor displayed high sensitivity, fast response, and reliable signal reproducibility over a wide strain range, allowing the stable monitoring of diverse human motions. In addition, the hydrogel bioelectrode delivered high signal-to-noise ratios and superior signal quality in the acquisition of ECG and EMG signals. This work provides an effective strategy for constructing high-performance ionically conductive hydrogels with wide applications in flexible electronics.

Conflict of Interests

The authors declare no interest conflict.

Electronic Supplementary Information

Electronic supplementary information (ESI) is available free of charge in the online version of this article at http://doi.org/10.1007/s10118-026-3571-3.

Data Availability Statement

The data that support the findings of this study are available upon request from the corresponding authors.

ACKNOWLEDGMENTS

This work was financially supported by the National Natural Science Foundation of China (Nos. 22102139 and 22372143) and Hebei Natural Science Foundation (Nos. B2025203022 and B2025203050), Science Research Project of the Hebei Education Department (No. JCZX2026028).

REFERENCES

1 Tang, X.; Qi, C.; Sun, Q. Recent progress of biosensors based on thermoelectric effects for monitoring physical activity and environment monitoring. *Soft Sci.* **2025**, *5*, 11.
2 Yang, W.; Liu, F.; Lin, Y.; Wang, J.; Zhang, C.; Cheng, H.; Chen, H. MXene-based flexible sensors for wearable applications. *Soft Sci.* **2025**, *5*, 33.
3 Wei, Y.; He, Y.; Wang, C.; Chen, G.; Zhao, B. Asymmetric "Janus" Biogel for Human-Machine Interfaces. *Adv. Func. Mater.* **2023**, *33*, 2214366.
4 Sun, Y.; Li, D.; Yang, R.; Zhou, Z.; Ji, T.; Lu, B.; Sun, L.; Liu, H. The Touch-Code Glove: a multimodal mapping interface with triboelectric-digital encoding for intuitive robot training. *Energy Mater.* **2025**, *5*, 60.
5 Zhao, Y.; Zhang, X.; Hao, Y.; Zhao, Y.; Ding, P.; Zhai, W.; Dai, K.; Zheng, G.; Liu, C.; Shen, C. Multifunctional PVA/PNIPAM conductive hydrogel sensors enabled human-machine interaction intelligent rehabilitation training. *Adv. Compos. Hybrid Ma.* **2024**, *7*, 245.
6 Wang, W.; Ma, Z.; Hu, Z.; Long, Y.; Wu, F.; Huang, X.; Nisa, F. u.; Liang, H.; Dong, Y.; Wang, J.; Tahir, M.; Xu, J.; He, L. Synergistic enhancement of hole–bridge structure and molecular-crowding effect in multifunctional eutectic hydrogel strain/pressure sensor for personal rehabilitation training. *Adv. Funct. Mater.* **2025**, *35*, 2502844.
7 He, Y.; Xu, X.; Xiao, S.; Wu, J.; Zhou, P.; Chen, L.; Liu, H. Research progress and application of multimodal flexible sensors for electronic skin. *ACS Sensors* **2024**, *9*, 2275.
8 Li, W.; Zheng, S.; Zou, X.; Ren, Y.; Liu, Z.; Peng, W.; Wang, X.; Liu, D.; Shen, Z.; Hu, Y.; Guo, J.; Sun, Z.; Yan, F. Tough hydrogels with isotropic and unprecedented crack propagation resistance. *Adv. Funct. Mater.* **2022**, *32*, 2207348.

Graphical Abstract

Interface-engineered Ionically Conductive Polyoxometalate-based Hydrogels with High Stretchability and Notch-insensitivity for Wearable Sensors

Xiao-Jiao Shi, Yu-Bin Zhang, Na Li, Yu-Xuan Qiao, Ya Liang, Gong-Kuo Yu, Ai-Hong Su, Ze-Cheng Song, Dan-Dan Song, Ti-Feng Jiao, and Zhi-Hui Qin

Yanshan University

A tough and notch-insensitive conductive hydrogel is developed by introducing L-arginine-regulated polyoxometalate nano-crosslinking domains. The hydrogel exhibits high stretchability, robust ionic conductivity, and sensitive strain sensing, enabling stable electrocardiogram (ECG) and electromyography (EMG) signal monitoring for wearable bioelectronics.

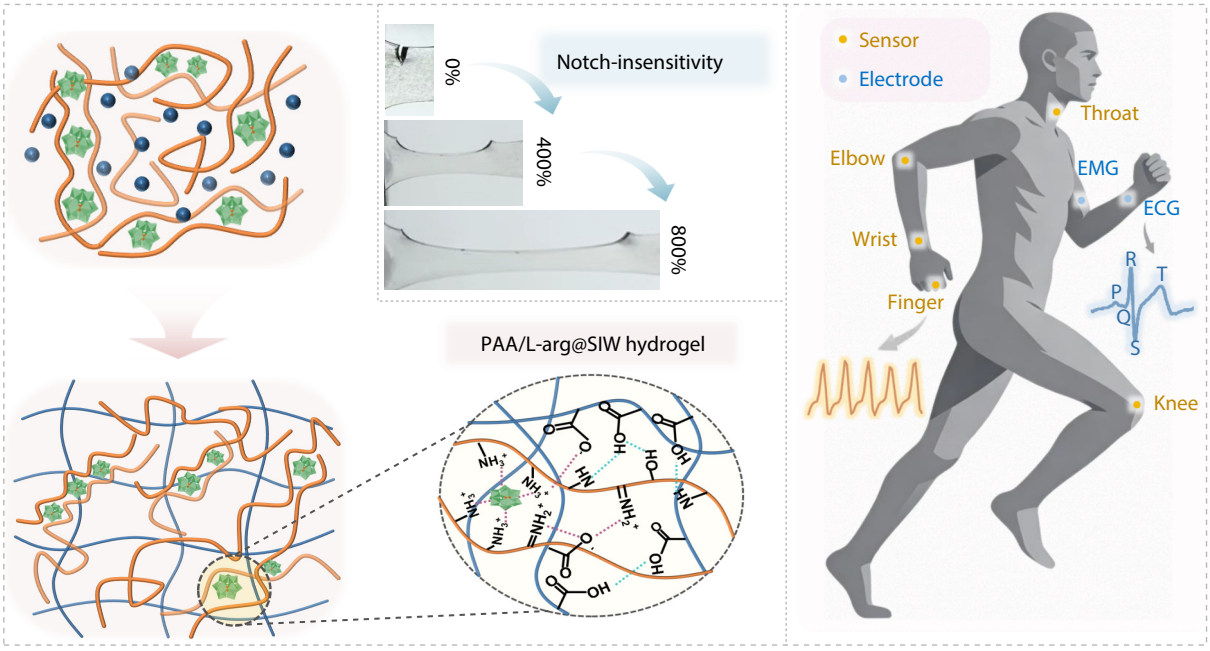

Chinese J. Polym. Sci., 2026 *https://doi.org/10.1007/s10118-026-3571-3*

9 Liu, Y.; Omar, R.; Li, G.; Zhou, P.; Zhang, Y.; Yan, W.; Haick, H.; Guo, C. F.; Someya, T.; Wang, Y. Adaptable conductive hydrogel-enabled soft electronics. *Prog. Mater Sci.* **2026**, *157*, 101590.

10 Xue, C.; Zhao, Y.; Liao, Y.; Zhang, H. Bioinspired super-robust conductive hydrogels for machine learning-assisted tactile perception system. *Adv. Mater.* **2025**, *37*, 2416275.

11 Sedlačík, T.; Nonoyama, T.; Guo, H.; Kiyama, R.; Nakajima, T.; Takeda, Y.; Kurokawa, T.; Gong, J. P. Preparation of tough double- and triple-network supermacroporous hydrogels through repeated cryogelation. *Chem. Mater.* **2020**, *32*, 8576.

12 Li, W.; Wang, X.; Liu, Z.; Zou, X.; Shen, Z.; Liu, D.; Li, L.; Guo, Y.; Yan, F. Nanoconfined polymerization limits crack propagation in hysteresis-free gels. *Nat. Mater.* **2024**, *23*, 131.

13 Wang, Y.; Chai, J.; Wang, H.; Xiao, T.; Zhao, J.; Chen, L.; Lei, W.; Liu, M. Solvent-mediated microphase separation in ionogels for the construction of mechanically robust and high-energy-output moisture-electric generators. *Interdisciplinary Materials* **2025**, *4*, 869.

14 Deng, Z. H.; Li, R. Q.; Deng, Q.; Zhu, D. Y.; Chen, W.; Chen, Z. P.; Zeng, Y. Z.; Qiu, X. Lego assembly-inspired self-healing hydrogels *via* lignin-mediated multi-dynamic cross-linking and slide-ring structure for adaptive sensors. *Macromolecules* **2025**, *58*, 8762.

15 Li, N.; Wang, X.; Liu, Y.; Li, Y.; Li, J.; Qin, Z.; Jiao, T. Ultrastretchable, self-adhesive and conductive MXene nanocomposite hydrogel for body-surface temperature distinguishing and electrophysiological signal monitoring. *Chem. Eng. J.* **2024**, *483*, 149303.

16 Gu, Y.; Xu, C.; Wang, Y.; Luo, J.; Shi, D.; Wu, W.; Chen, L.; Jin, Y.; Jiang, B.; Chen, C. Compressible, anti-fatigue, extreme environment adaptable, and biocompatible supramolecular organohydrogel enabled by lignosulfonate triggered noncovalent network. *Nat. Commun.* **2025**, *16*, 160.

17 Qiao, S.; Yang, X. C.; Wang, X.; Yu, S. S.; Yu, X.; Chen, K. Z. Sacrificial bond-enabled mechanically robust, stretchable ionic hydrogels for high-performance wearable sensors. *Chem. Eng. J.* **2025**, *525*, 170049.

18 Li, C.; Sun, Y.; Li, Y.; Jiao, C.; Fu, X.; Zhou, X.; Li, Z.; Ling, S.; Ye, D.; Zheng, K. Biomimetic interface engineering approach for

universal toughening of rigid fibers. *Adv. Funct. Mater.* **2025**, *35*, 2501380.
19 Mo, F.; Lin, Y.; Liu, Y.; Zhou, P.; Yang, J.; Ji, Z.; Wang, Y. Advances in ionic conductive hydrogels for skin sensor applications. *Mat. Sci. Eng.: R* **2025**, *165*, 100989.
20 Liu, S.; Lv, J.; Zhu, M.; Zhang, H.; Li, N.; Hu, Z.; Chen, S. Branch chain engineering inorganic nanofiller to construct high-performance inorganic-organic hybrid membrane. *J Membr. Sci.* **2025**, *733*, 124353.
21 Li, B.; Xuan, L.; Wu, L. Polyoxometalate-containing supramolecular gels. *Macromol. Rapid Commun.* **2022**, *43*, 2200019.
22 Wang, Z.; Liang, S.; Yang, Y.; Liu, Z. N.; Duan, X.; Li, X.; Liu, T.; Zang, H. Complex phase transitions and phase engineering in the aqueous solution of an isopolyoxometalate cluster. *Nat. Commun.* **2023**, *14*, 2767.
23 Gumerova, N. I.; Rompel, A. Synthesis, structures and applications of electron-rich polyoxometalates. *Nat. Rev. Chem.* **2018**, *2*, 0112.
24 Yang, P.; Zhao, W.; Shkurenko, A.; Belmabkhout, Y.; Eddaoudi, M.; Dong, X.; Alshareef, H. N.;Khashab, N. M. Polyoxometalate–cyclodextrin metal–organic frameworks: from tunable structure to customized storage functionality. *J. Am. Chem. Soc.* **2019**, *141*, 1847.
25 Du, L.; Chen, Y.; Zhao, X.; Ren, X.; Wang, G.; Wu, P.; Zhang, Y. Noncovalently crosslinked silk fibroin based double network hydrogels with adhesive and self-healing property for wound repair. *Colloid. Surface. B* **2025**, *256*, 114981.
26 Huang, S.; Xia, X. X.; Fan, R. X.; Qian, Z. Programmable electrostatic interactions expand the landscape of dynamic functional hydrogels. *Chem. Mater.* **2020**, *32*, 1937.
27 Ma, M.; Li, C.; Fan, W.; Su, Y.; Guo, D.; Li, M.; Zhou, Y. Constructing high-efficiency polyoxometalate-based antibacterial hydrogels for wearable sensors. *Langmuir* **2025**, *41*, 26261.
28 Su, H.; Zhang, Z.; Song, W.; Shi, K.; Cheng, F.; Hao, M.; Ma, Y.; Chen, Y.; Wu, G.; Song, Y. A double network AG/P(AAm-AAc)/P2W18 hydrogel with high stretchability for flexible electrochromic device. *Eur. Polym. J.* **2024**, *204*, 112705.
29 Bielański, A.; Datka, J.; Gil, B.; Małecka-Lubańska, A.; Micek-Ilnicka, A. FTIR study of hydration of dodecatungstosilicic acid. *Catal. Lett.* **1999**, *57*, 61.
30 Yang, J.; Zhang, L.; Wang, Y.; Wang, N.; Wei, H.; Zhang, S.; Ding, Q.; Sun, S.; Ding, C.; Liu, W. Dihydromyricetin-loaded oxidized polysaccharide/L-arginine chitosan adhesive hydrogel promotes bone regeneration by regulating PI3K/AKT signaling pathway and MAPK signaling pathway. *Carbohydr. Polym.* **2024**, *346*, 122614.
31 Heydari, P.; Varshosaz, J.; Kharaziha, M.; Javanmard, S. H. Antibacterial and pH-sensitive methacrylate poly-L-Arginine/poly (β-amino ester) polymer for soft tissue engineering. *J Mater. Sci. Mater. M* **2023**, *34*, 16.
32 Xu, J.; Li, X.; Li, J.; Li, X.; Li, B.; Wang, Y.; Wu, L.; Li, W. Wet and functional adhesives from one-step aqueous self-assembly of natural amino acids and polyoxometalates. *Angew. Chem. Int. Ed.* **2017**, *56*, 8731.
33 Song, Y.; Li, H.; Shan, T.; Yang, P.; Li, S.; Liu, Z.; Liu, C.; Shen, C. MOF-implanted poly (acrylamide-co-acrylic acid)/chitosan organic hydrogel for uranium extraction from seawater. *Carbohydr. Polym.* **2023**, *302*, 120377.
34 Radwan, R. R.; Mohamed, H. A.; Ali, H. E.; Mahmoud, G. A. Radiation preparation of l-arginine/acrylic acid hydrogel matrix patch for transdermal delivery of propranolol HCl in hypertensive rats. *Drug Deliv. Transl. Re.* **2018**, *8*, 525.
35 Bajuk-Bogdanović, D.; Uskoković-Marković, S.; Holclajtner-Antunović, I. Vibration spectroscopy stability investigation of 12-tungstosilicic acid Solution. *J. Iran. Chem. Soc.* **2015**, *12*, 137.
36 Sukiasyan, R. P.; Suponitsky, K. Y.; Atanesyan, A. K.; Danghyan, A. A.; Hovhannisyan, A. A.; Petrosyan, A. M. Crystal structures and vibrational spectra of L-argininium(2+) bis(tetrafluoroborate) and L-argininium(2+) bis(perchlorate). *Spectrochim. Acta A* **2020**, *228*, 117782.
37 Todica, M.; Stefan, R.; Cornel, P.; Olar, L. IR and Raman investigation of some poly(acrylic) acid gels in aqueous and neutralized state. *Acta Phys. Pol., A* **2015**, *128*, 128.
38 Xue, S.; Lu, Y.; Geng, J.; Yang, J.; Zhu, M.; Bai, X.; Liu, S. Polyoxometalate-based self-adhesive hydrogels with both proton conductive and photochromic functions. *J. Mater. Chem. C* **2025**, *13*, 11319.
39 Yang, J.; Chen, M.; Li, P.; Cheng, F.; Xu, Y.; Li, Z.; Wang, Y.; Li, H. Self-healing hydrogel containing Eu-polyoxometalate as acid-base vapor modulated luminescent switch. *Sensors Actuat. B Chem.* **2018**, *273*, 153.
40 Pruksawan, S.; Lim, J. W. R.; Lee, Y. L.; Lin, Z.; Chee, H. L.; Chong, Y. T.; Chi, H.; Wang, F. Enhancing hydrogel toughness by uniform cross-linking using modified polyhedral oligomeric silsesquioxane. *Commun. Mater.* **2023**, *4*, 75.
41 Xu, Z.; Chen, Y.; Cao, Y.; Xue, B., Tough hydrogels with different toughening mechanisms and applicationsin. *Int. J Mol. Sci* **2024**, 25, 2675.
42 Li, W.; Li, L.; Liu, Z.; Zheng, S.; Li, Q.; Yan, F. Supramolecular Ionogels Tougher than Metals. *Adv. Mater.* **2023**, *35*, 2301383.
43 Guo, X.; Zhang, S.; Patel, S.; Sun, X.; Zhu, Y.; Wei, Z.; Wang, R.; He, X.; Wang, Z.; Yu, C.; Tan, S. C. A skin-mimicking multifunctional hydrogel *via* hierarchical, reversible noncovalent interactions. *Sci. Adv.* **2025**, *11*, eadv8523.
44 Yang, Y.; Sun, H.; Shi, C.; Liu, Y.; Zhu, Y.; Song, Y. Self-healing hydrogel with multiple adhesion as sensors for winter sports. *J. Colloid Interface Sci.* **2023**, *629*, 1021.
45 Chong, J.; Sung, C.; Nam, K. S.; Kang, T.; Kim, H.; Lee, H.; Park, H.; Park, S.; Kang, J. Highly conductive tissue-like hydrogel interface through template-directed assembly. *Nat. Commun.* **2023**, *14*, 2206.
46 Wei, X.; Ma, K.; Cheng, Y.; Sun, L.; Chen, D.; Zhao, X.; Lu, H.; Song, B.; Yang, K.; Jia, P. Adhesive, conductive, self-healing, and antibacterial hydrogel based on chitosan–polyoxometalate complexes for wearable strain sensor. *ACS Appl. Polym. Mater.* **2020**, *2*, 2541.
47 Shi, X.; Xu, L.; Xu, Q.; Li, N.; Li, X.; Zhang, Y.; Qin, Z.; Jiao, T. Ultrasoft conducting polymer hydrogels with large biaxial strain and conformal adhesion for sensitive flexible sensors. *Chem. Mater.* **2024**, *36*, 10560.
48 Li, Q.; Tian, B.; Tang, G.; Zhan, H.; Liang, J.; Guo, P.; Liu, Q.; Wu, W. Multifunctional conductive hydrogels for wearable sensors and supercapacitors. *J. Mater. Chem. A* **2024**, *12*, 3589.